Analytica Chimica Acta 1055 (2019) 7–16

Contents lists available at ScienceDirect

Analytica Chimica Acta

journal homepage: www.elsevier.com/locate/aca

Sub-femtomolar detection of HIV-1 gene using DNA immobilized on composite platform reinforced by a conductive polymer sandwiched between two nanostructured layers: A solid signal-amplification strategy

Mojtaba Shamsipur*, Leila Samandari, Avat (Arman) Taherpour, Afshin Pashabadi

Department of Chemistry, Razi University, Kermanshah, Iran

HIGHLIGHTS

- A solid-signal amplification strategy is studied.
- A ternary polymer-sandwiched composite has been constructed as a biosensor platform.
- The fabricated sensor revealed an exclusive performance toward the HIV-gen.
- A single frequency strategy has been exploited to perform a rapid impedance transducing procedure.

GRAPHICAL ABSTRACT

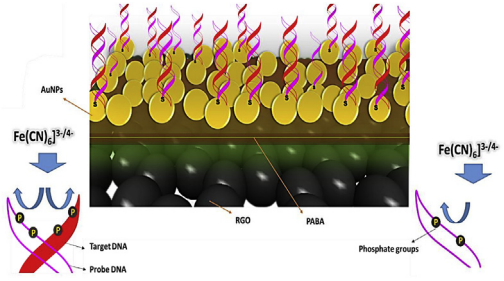

ARTICLE INFO

Article history:
Received 3 September 2018
Received in revised form
25 November 2018
Accepted 7 December 2018
Available online 29 December 2018

Keywords:
Human immunodeficiency virus
DNA biosensor
Impedimetry
Composite electrode
Density functional theory

ABSTRACT

This study introduces a signal amplification strategy rely on incorporating a specific polymer film between two typical nanostructured layers, aiming to improve the electrical properties of the platform to be able to transduce small binding event through sub-femtomolar detection of HIV-1 gene at the surface of the constructed biosensing device. The proposed composite was arrayed based on a conductive layer consist of *p*-aminobenzoic acid (PABA) sandwiched between the electrochemically reduced graphene oxide (ERGO) as the sub-layer, and the gold nanoparticles (AuNPs) as the interfacial layer. We computationally explored that how the use of such design enables the platform to transduce small changes in the interfacial properties of the biosensor, caused by low concentrations of HIV-1 gene, without needing any amplification strategy. Furthermore, it was found that the loin PABA conductive polymer sandwiched between two nanostructure layers play an artwork-ensemble role, which resulted in a good signal repeatability and stability during the relatively long successive incubation and detection procedures. The justification of using such an array of conductive layers was established on the attaining extra low-level of detection limit. The observed performance for probe-DNA immobilized on glassy carbon electrode (GC) modified with ERGO/PABA/AuNPs compared to the GC electrode modified with ERGO/AuNPs inspired us to perform computational calculations, a hybrid of *ab-initio* and semi-empirical quantum mechanics methods, to discover its probable molecular-scale reasons. A rapid single frequency impedance measurement (SFIM) was also employed to remarkably reduce the measurement time and diminish the probable nonspecific impedance changes. The proposed biosensor was used to evaluate the DNA

* Corresponding author. Faculty of Chemistry, Department of Analytical Chemistry, Razi University, Kermanshah, Iran.
E-mail address: mshamsipur@yahoo.com (M. Shamsipur).

https://doi.org/10.1016/j.aca.2018.12.013

target over an extremely wide concentration range from 0.1 fM to 10 nM, with a detection limit of 37 aM (S/N = 3).

1. Introduction

Human immunodeficiency virus (HIV) is a retrovirus that attacks the host's immune system, destroys the T4 lymphocytes, causes breakdown of the human's immune system and finally results in death. Thus, monitoring of HIV biomarker or gene has become critically important for the early diagnosis, clinical therapy and prevention of virus's propagation [1]. HIV-1 and HIV-2 are the two major types of HIV. The first case is responsible for 95% of all HIV infections worldwide.

Various experimental methods have already been reported for monitoring and quantifying of the HIV-1 [1]. Currently, the most frequently used method for the early diagnosis of this virus is based on immunoassay approach [2–5]. However, it needs several weeks to several months for HIV's infection and HIV antibodies' production, named as HIV's window period. The Western blot assay, a couple of radio-isotopic detection with electrophoretic separation, was also designated for this task [6], although, this procedure is time consuming, tedious and is indeed an end-point determination method. Moreover, in recent years, DNA hybridization schemes [7] have attracted considerable attentions for monitoring HIV-1 DNA sequences [8–10].

Since DNA biomarkers associated with most diseases have low-abundant in the human body, which prevent using most of the proposed methods in real samples analyses. Therefore, it is important to develop ultrasensitive biosensors for DNA detection, the issue that inspired researchers to establish various innovative procedures based on DNA amplification for ultrasensitive sequence-specific detection of DNA. Majority of these methods relied on polymerase chain reaction (PCR) [11], nucleic-acid sequence-based amplification (NASBA) [12] and rolling circle amplification (RCA) [13], the amplification strategies that are costly and require special tools, tedious labels and complex operations. In this way, the electrochemical based biosensing systems have been widely used for DNA detection due to their high sensitivity, simplicity, portability, rapidness and low cost. In order to improve sensitivity of electrochemical DNA biosensors, different nanomaterials, such as metal nanoparticles [14], carbon-based nanostructures [15], graphene sheets [16] and conducting polymers [17] have been utilized.

Due to their specific physical and chemical properties such as high stability and selectivity, good reproducibility, homogeneity, and strong adherence to the electrode surface, the electrodes modified with conducting polymers have been the subject of increasing interest in recent years [18]. These characteristics have made them potential candidates for application in various fields of electrochemistry including; energy storage [19], electrocatalysis [20] and sensing devices [21]. *P*-Aminobenzoic acid (PABA) contains the electron-rich N atom and high electron density carbonyl group, which is easy to be electropolymerized on glassy carbon electrode via potential cycling. In recent years, PABA polymeric films have been used in constructing different electrochemical sensing devices [22–25]. In most of these reports, exploiting PABA induced high stability and robustness in the performance of extended composite electrodes.

This work represents an impedimetric DNA-based biosensor able to quantify sub-femtomolar of HIV-1 pol gene based on a simple detection route without needing any amplification strategy. Inspired by the comparative results of impedance experiments toward the target-DNA, we performed computational calculations, a hybrid of *ab-initio* and semi-empirical QM methods, to find a reasonable response for the observed signal amplification upon incorporating PABA in the composite framework of the fabricated biosensor. We have recently reported multiple electrochemical research works that exploited computational modeling and density functional theory (DFT) to study some superior catalytic performances and also to explore the electrical characteristics of the extended composite electrodes [26–32]. Comparing the analytical response of the constructed biosensor based on a sandwiched array (ssDNA/AuNPs/PABA/ERGO/GCE) with the ssDNA/AuNPs/ERGO/GCE disclosed a supreme performance for the polymer sandwiched architecture, while the electrochemical measurements showed a slight increase in effective surface area calculated for AuNPs/PABA/ERGO/GCE platform compared to that for AuNPs/ERGO/GCE. Such comparison specified that negligible change in effective surface area solely could not justifies the significant signal amplification occurred upon incorporating PABA into the composite body, the fact that motivated us to establish a computational study to ascertain the main factor involved in this exclusive behavior. The results of calculation exposed that composing PABA into the sensing layer significantly decreased the HOMO-LUMO gap of the modeled structure, allowing the composite to transduce smaller change in electronical properties occurred by a low concentration of target DNA toward the surface-immobilized recognition element (probe DNA) at the interface of electrode/electrolyte. In brief, this research represents a solid-signal amplification strategy by incorporating a PABA layer to transduce lower signal change caused by low concentration of analyte at the interface of electrode electrolyte by faradic impedance spectroscopy (FIS). The report also testified using a single frequency impedance measurement (SFIM) allowed us to quantitatively monitor ultra-traces of the analyte with good repeatability at a short time ranges; a coupled strategy that will be effective during designing diverse impedimetric biosensing devices for sensitive and rapid detection of low concentration of different analytes.

2. Experimental

2.1. Reagents and chemicals

All chemicals were of analytical reagent grade and used without further purification. Extra pure graphite powder, sodium dihydrogen phosphate (NaH_2PO_4), sodium hydrogen phosphate (Na_2HPO_4), potassium chloride (KCl), potassium hexacyanoferrate (III) ($K_3[Fe(CN)_6]$ and potassium hexacyanoferrate(II) ($K_4[Fe(CN)_6]$) were obtained from Merck (Darmstadt, Germany). *Para*-Aminobenzoic acid (PABA) and sodium tetrachloroaurate (III) dihydrate ($NaAuCl_4 \cdot 2H_2O$) were obtained from Sigma-Aldrich (St. Louis, MO, USA). Double distilled water was used in all experiments. The probe DNA, its target (conserved sequence of the HIV-1 pol gene fragment), double base mismatched, four-base mismatched and non-complementary with the following sequences were all obtained from Faza Biotech Co. (Tehran, Iran):

Probe DNA (ssDNA): 5′-SH-GCT TGC CAA TGA TCT GTC CA-3′

Target DNA: 5′-TGG ACA GAT CAT TGG CAA GC-3′

Double-base mismatched DNA: 5′-TGG ACA AAT CAT CGG CAA GC-3′

Four-base mismatched DNA: 5′-TGT ACA AAT CAT CGG CAG GC-3′

Non-complementary DNA: 5′-CAT CTC ATG GCC GAT TCG TG-3′.

2.2. Apparatus and measurements

The electrochemical measurements were carried out with a μ-Autolab type III (Eco Chemie B·V.A) computer-controlled potentiostat and running with GPES and FRA softwares coupled with a conventional three-electrode cell: Ag/AgCl/KCl (3 M) as a reference electrode, platinum wire as an auxiliary electrode and modified GCE (2 mm in diameter, Azar Electrode, Urmia, Iran) as a working electrode. Electrochemical impedance spectroscopic measurements were run in 5 mM of $K_3[Fe(CN)_6]/K_4[Fe(CN)_6]$ containing 0.1 M KCl. The EIS measurements frequency range was chosen from 10^5 to 0.01 Hz and the Ac voltage amplitude was 10 mV. All electrochemical measurements were performed at room temperature (25 ± 1 °C).

Field Emission Scanning Electron Microscopy (FESEM) images were obtained using TESCAN MIRA3 LMU. FTIR spectra were recorded on a Bruker ALPHA spectrometer (Germany). UV–Vis absorption spectra were recorded using an Agilent spectrophotometer (8453, Santa Clara, CA, USA).

2.3. Preparation of AuNPs/PABA/ERGO/GCE

Graphene oxide (GO) was prepared by oxidizing natural graphite powder using a modified Hummers' method [33,34]. The graphene oxide suspension (1 mg mL^{-1}) was prepared by dispersing 1.0 mg of graphene oxide in 1.0 mL of deionized water and irradiated in the ultrasonic bath for 30 min. Before modification, the surface of bare GCE was polished to a mirror-like surface with 0.3, 0.1 and 0.05 μm alumina powders (Struers, Denmark) and then cleaned in a water-ethanol solution (1:1) under ultrasonication. The electrode was electrochemically cleaned also through cycling in the solution of 0.1 M H_2SO_4 over a potential range of −0.2–1.4 V until a reproducible CV was obtained [35]. Finally, the electrode washed with ultrapure water and dried. 3 μL of GO was dropped on its surface and allowed to dry at air. The GO/GCE was then transferred to an electrochemical cell containing 0.1 M phosphate buffer solution (PBS, pH = 5) and 30 successive cyclic voltammograms were conducted in the potential range between 0.0 and −1.5 V at the scan rate of 50 mV s^{-1} to form the electrochemically reduced graphene oxide modified glassy carbon electrode (ERGO/GCE). After rinsing with ultrapure water, the electropolymerization of PABA on ERGO/GCE was performed in 0.1 M PBS (pH = 7.0) containing 1.0 mM of PABA by cyclic potential scanning from −1.5 to 2.5 V for 6 cycles at a scan rate of 30 mV s^{-1} [36]. For the deposition of AuNPs, the fabricated PABA/ERGO/GCE was transferred into the electrochemical cell containing 5 mM $NaAuCl_4 \cdot 2H_2O$ and 12 successive CV cycles was applied over the potential range between 0.1 and −1.2 V at a scan rate of 50 mV s^{-1}. In the subsequent step, 5 μL of 1 μM of the capture probe was dropped on the surface of the composite electrode and allowed to stay for 16 h at 4 °C in the refrigerator. During the assay experiments, the hybridization reaction was conducted by dropping 5 μL of the fixed concentration of target HIV gene solution onto the biosensor surface and allowed to react for the optimized time of 1 h. Subsequently, the electrode was rinsed with PBS of pH 7.0 to remove the un-hybridized target strands. The same procedure was applied for hybridization of the double-base mismatched, four base mismatched and non-complementary DNA sequences. The concentrations of these sequences were all selected as 0.1 nM.

3. Results and discussion

3.1. Preparation and characterization of the composite film

Fig. S1 shows the cyclic voltammograms for the formation of PABA film that was recorded in the solution of 1.0 mM of monomer in pH 7.0 (PBS) at the surface of ERGO/GCE. As it is shown, by increasing number of cycles, two anodic peaks emerged at 0.15 and 1.64 V together with two corresponding reduction peaks at 0.34 and −0.62, *vs.* Ag/AgCl, indicating deposition of PABA on ERGO through the electropolymerization process [25]. After drying PABA/ERGO/GCE in the air, the visual inspection of the fabricated film displayed the deposition of a dark-blue film. Since the film was not dissolved upon successive anodic and cathodic sweeps, it could be concluded that the deposited film is a polymeric material [27].

The prepared GO was characterized by using FTIR and UV–Vis spectroscopy. The UV–Vis spectrum which is shown in Fig. S2, displayed an absorption peak at 230 nm that could be attributed to the π-π* transition of aromatic C=C bonds. Another shoulder at *ca.* 300 nm was ascribed to the n→π* transition of the C=O bonds [37,38]. The FT-IR spectrum of GO/GCE and ERGO/GCE are shown in Fig. S3. The FT-IR spectrum recorded for GO (curve a) shows the hydroxyl and epoxy vibrational bands at 3450 and 1201 cm^{-1}, respectively. The characteristic peaks at 1670 and 1043 cm^{-1} are assigned to the stretching vibration of C–O (epoxy) and stretching of C–O (alkoxy) respectively. In the ERGO FTIR spectrum (curve b), some peaks related to the oxygen disappeared and the intensities of other pecks significantly decreased, which indicate the electrochemical reduction of GO. In addition, to further illustrate the reduction of GO, Raman spectroscopy was used. Based on the literature, there are two main bands for Graphene base material including D and G bands. By reducing graphene oxide, the intensity of D/G is increased [39] (see Fig. S5), which confirms the electrochemical reduction of graphene oxide. To display the successful electropolymerization of PABA, the attenuated total reflection (ATR) was taken for the PABA electropolymerized on the GCE. Its result is shown in Fig. S5 curve a (In order to diminish the spectral interference, the ERGO was removed from the sub-layer). For comparison, the IR spectra was recorded for the monomer of *p*-ABA, which the result is shown in Fig. S5 curve d. The main differences between the IR spectra of the monomer and the polymer are vibration bands of the amino groups, where, the sharp (N–H) bands located around 3600~3300 cm^{-1} of monomer are relatively diminished and changed to a broad wave [40]. Moreover, the strong band at 1692 cm^{-1} is assigned to the presence of (C=O) group [40,41].

Fig. 1 displays the FESEM and EDX characterization taken for different deposited layers on GCE. The ERGO film on the electrode surface (Fig. 1A) exhibits a typical wrinkled and crumpled structure which is in agreement with the formation of ERGO at the surface of GCE [42]. The morphology of subsequent composed layers including PABA/ERGO/GCE (Fig. 1B) and AuNPs/PABA/ERGO/GCE (Fig. 1C) were examined by FESEM and signified the formation of nanosized islands of the conductive polymer PABA, followed by the deposition of the AuNPs with the average size of about 75 nm as the interfacial-layer of the composite electrode. The energy-dispersive X-ray spectroscopy (EDX) (Fig. 1D) and scanning electron microscopy/energy dispersive X-ray spectroscopy (SEM/EDX) (Fig. 1E) clearly showed the presence of different percentages of Au, S, O, N and C at the prepared biosensing layer.

3.2. Electrochemical characterization of the DNA biosensor

In this work, we concentrated our attention on developing a simple biosensing device, without needing any amplification

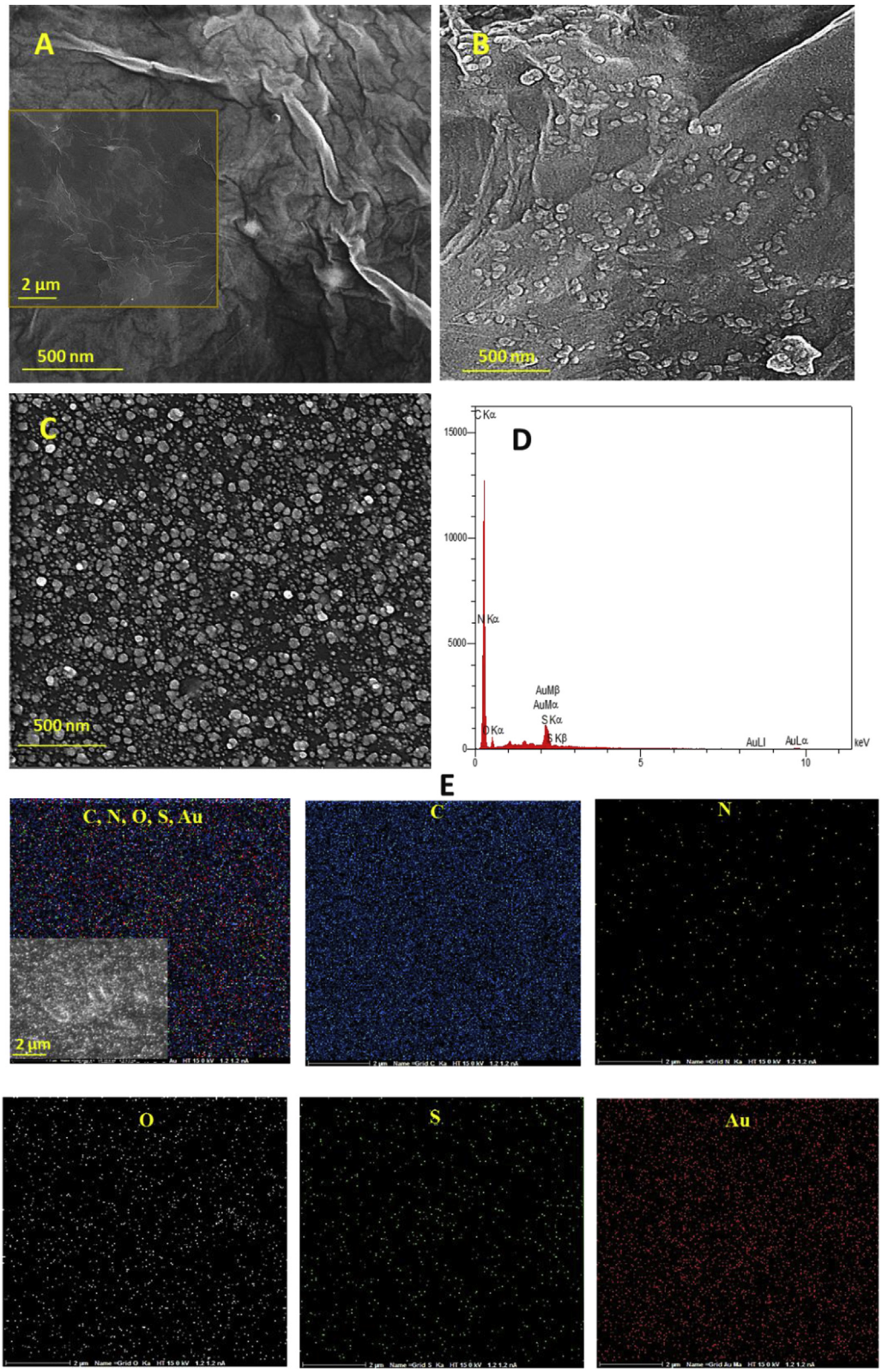

Fig. 1. The FESEM images of ERGO/GCE (A), PABA/ERGO/GCE (B), AuNPs/PABA/ERGO/GCE (C), The EDX spectrum of ssDNA/AuNPs/PABA/ERGO/GCE (D), EDX mapping of modified electrode, showing signals of carbon, oxygen, nitrogen, sulfur and Au (E).

approaches, to detect low-level of HIV-1 pol gene. This work aimed to avoid using any complicate strategy in sensing and transducing of occurred events caused by the interaction of probe DNA and target DNA. In this regard, during preliminary studies, a reputable coupled nanostructured layer composing reduced graphene oxide and gold nanoparticle, which delivered the exclusive surface-to-volume and exclusive electron transfer properties in constructing electrochemical sensing devices, was utilized to immobilize the probe DNA on the transducer. Afterward, the capability of the constructed biosensor based on AuNPs/ERGO/GCE was verified in detecting low-level of HIV-1. As you can see in Fig. 2 (curves a, b, c) the corresponding results revealed no significant signal change toward target DNA. In further stages of the work, after more studies and performing some early DFT calculations, *p*-aminobenzoic acid (PABA), as a gold-tended monomer [43], was electropolymerized on the ERGO sub-layer and sandwiched by the electrodeposition of AuNPs interfacial layer to form the AuNPs/PABA/ERGO/GCE platform. Interestingly, the results of the experiments shown in Fig. 2 (curves d, e, f) confirmed our primary prediction about its remarkable influence of sandwiched layer on the capability of the composite platform for the detection of extra-small changes occurred in the electrical properties of interfacial layer [28]; as was appeared in the exclusive ability of the biosensor toward sub-femtomolar concentration of HIV-1 by electrochemical impedance spectroscopy (EIS). The use of PABA as a reinforcing layer in the composite layer lead to the significant enhancement in the analytical signal. In other words, the induced strength by PABA resulted in robust response during relatively usual long detection procedure employed, including incubation and signal recording, in impedimetric biosensing of HIV-1 pol gene.

The electroactive surface area (A) for GCE, AuNPs/ERGO/GCE, and AuNPs/PABA/ERGO/GCE was evaluated from the cyclic voltammograms recorded in the solution of 5 mM of $K_3[Fe(CN)_6]$ containing 0.1 M KCl at various sweep rates. The calculation was performed using the Randles-Sevcik equation [44]:

$$I_p = (2.69 \times 10^5)\, n^{3/2} A C D^{1/2} \upsilon^{1/2} \quad (1)$$

Where, Ip refers to the anodic peak current, $n = 1$ and $D = 7.6 \times 10^{-6}\ cm^2\ s^{-1}$ (in 0.1 M KCl). According to this equation, the effective surface areas were estimated from the slope of the linear plots of I_{pa}–$\upsilon^{1/2}$, as 0.040, 0.087 and 0.115 cm^2 for bare GCE, AuNPs/ERGO/GCE, and AuNPs/PABA/ERGO/GCE, respectively. It was found that the electroactive surface area after incorporation of PABA film is spatially increased, the relatively small changes in the effective surface area (*ca.* 30%) that specifically could not be the only reason for the significant improvement in the response of biosensors constructed based on AuNPs/PABA/ERGO/GCE compared to that on AuNPs/ERGO/GCE. Therefore, we particularly employed DFT calculations (see section 3.3.) to investigate more possible reasons for such performance, to be helpful in further work in future to select knowingly novel materials to improve the performance of electrochemical sensing devices.

Electrochemical impedance spectroscopy (EIS) is well established as one of the effective techniques to describe the interfacial properties of the biosensor fabrication and binding processes. Thus, in the next step, we recorded the Nyquist plots in 5.0 mM of $[Fe(CN)_6]^{3-/4-}$ at bare GCE (a), ERGO/GCE (b), PABA/ERGO/GCE (C) and AuNPs/PABA/ERGO/GCE (d). The curves e and f show respectively the equivalents Nyquist plots recorded after binding of ssDNA and dsDNA on the surface of the composite electrode (Fig. 3). The obtained impedance curves displayed identical depressed-semicircular, signifying capacitance dispersion, the Nyquist plots with a straight-line portion at lower frequencies. The semicircles show a combination of double layer capacitance and electron transfer resistance (R_{et}) in electrode/electrolyte interfaces on each modified electrode and represent the kinetically controlled movement of electrons. The diameter of semi-circles is proportional to the charge transfer resistance and can be used to directly evaluate the electron transfer properties of the electrode. The straight-line portion specifies the Warburg impedance, which takes in to account the frequency dependence on diffusion to the electrode surface. The R_{et} value for bare GC was 353Ω (curve a). When the electrode modified with ERGO (curve b), the R_{et} value decreased to 213Ω, which indicates good electron transfer of ERGO/GCE. After the electropolymerization of PABA on ERGO/GCE (curve c) the R_{et}

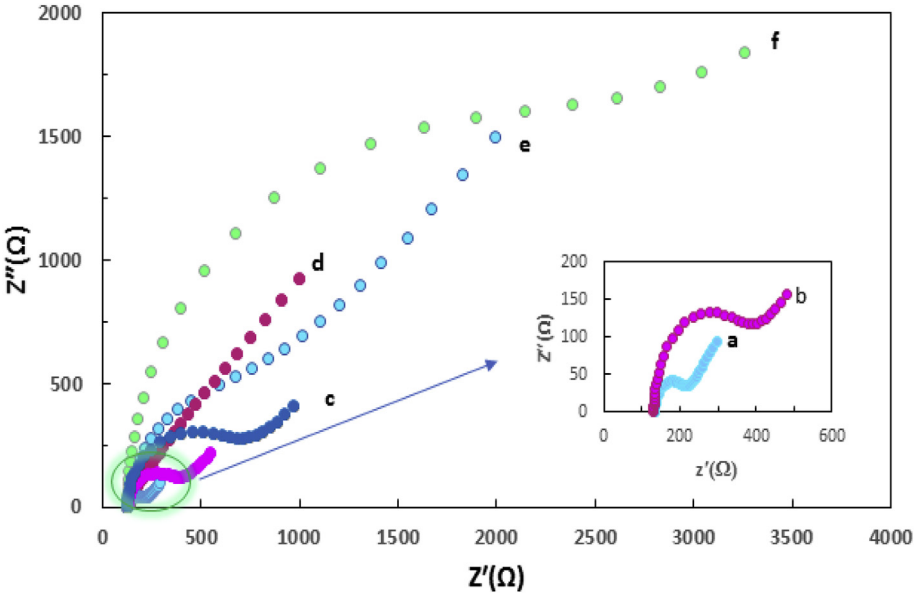

Fig. 2. Nyquist diagrams obtained at AuNPs/ERGO/GCE (a), ssDNA/AuNPs/ERGO/GCE (b), dsDNA/AuNPs/ERGO/GCE (c), AuNPs/PABA/ERGO/GCE (d) ssDNA/AuNPs/PABA/ERGO/GCE (e) dsDNA/AuNPs/PABA/ERGO/GCE (f). Conditions: 0.1 pM of HIV-1 pol gene in incubation solution in 5.0 mM $[Fe(CN)_6]^{3-/4-}$ solution containing 0.1 M KCl over frequency range of 10^5 to 0.01 Hz with $E_{ac} = 10$ mV.

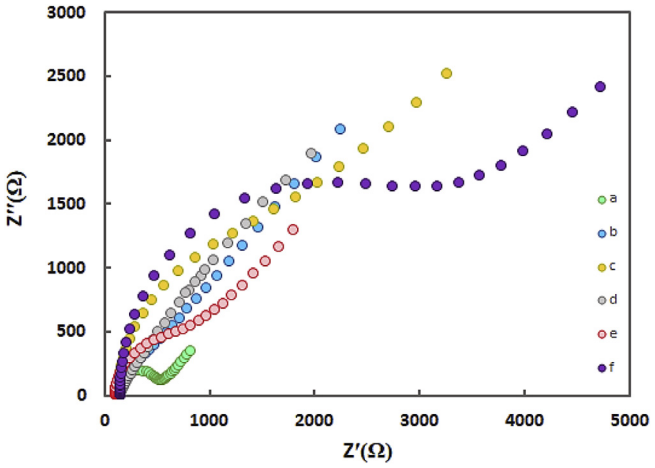

Fig. 3. Nyquist plots of impedance spectra for bare GCE(a), ERGO/GCE (b), PABA/ERGO/GCE (c) AuNPs/PABA/ERGO/GCE (d), ssDNA/AuNPs/PABA/ERGO/GCE (e), dsDNA/AuNPs/PABA/ERGO/GCE (f). Conditions: 0.1 pM of HIV-1 pol gene in incubation solution in 5.0 mM $[Fe(CN)_6]^{3-/4-}$ solution containing 0.1 M KCl over frequency range of 10^5 to 0.01 Hz with $E_{ac} = 10$ mV.

value increased to 1487Ω due to the low conductivity of the polymer film. Finally, after electrodeposition of AuNPs (curve d), the R_{et} decreased to 26 Ω, which shows the improvement of the electron transfer on the electrode. With immobilization ssDNA on the surface of the electrode (curve e), the R_{et} value increased to 589Ω. Finally, with incubation with target DAN, the R_{et} increased to 2638 Ω (curve f). The displayed curves appropriately confirm the successful formation of the composite platform, the immobilization of the probe DNA and hybridization of target DNA with the probe DNA. The impedance curves show increasing R_{et} for ssDNA/AuNPs/PABA/ERGO/GCE and dsDNA/AuNPs/PABA/ERGO/GCE after immobilization of ssDNA and, subsequently, those following signal changes caused by the interaction of target-DNA with ssDNA. The results appropriately evidenced immobilization of the probe DNA onto the composite electrodes with AuNPs interfaces, the event that makes difficult the electron transfer capability of redox-probe at the interface of electrode/electrolyte. This is mainly due to the presence of an electrostatic repulsive force between the negatively-charged ssDNA and the $[Fe(CN)_6]^{3-/4-}$. Finally, after the hybridization of 0.1 pM of target DNA, the R_{et} value further increased (curve f), signifying that the target-DNA is hybridized with the ssDNA at the surface of the biosensor to form dsDNA/AuNPs/ERGO/GCE.

In following, to consider the effect of incorporation of PABA on the biosensor response, we compared the results of the EIS curves obtained on the biosensors constructed based on AuNPs/GCE and AuNPs/PABA/GCE toward 0.1 pM of HIV pol gene (Fig. 4). It was found that the incorporation of PABA directly affects the sensitivity of biosensor, as the analytical signal changes revealed the values 155 Ω/0.1 pM and 1372 Ω/0.1 pM for ssDNA/AuNPs/GCE and ssDNA/AuNPs/PABA/GCE toward HIV^{-1} pol gene, respectively, which clearly demonstrates the profound effect of incorporation of PABA on the sensitivity of biosensor.

Further analysis of as prepared composited based biosensor was performed using cyclic voltammetry. Fig. S6 shows the cyclic voltammograms recorded at the GCE (a), AuNPs/PABA/ERGO/GCE (b), ssDNA/AuNPs/PABA/ERGO/GCE (c) and dsDNA/AuNPs/PABA/ERGO/GCE (d) in the presence of 5.0 mM of $[Fe(CN)_6]^{3-/4-} + 0.1$ M KCl. The bare GCE shows a pair of nearly reversible redox peaks with a peak-to-peak separation of $\Delta E = 94$ mV. When the electrode was modified as AuNPs/PABA/ERGO, the main feature of voltammogram is a significant increase in the current response, demonstrating that the AuNPs/PABA/ERGO nanocomposite possesses a higher effective surface area (curve b). After immobilization of ssDNA on the surface of AuNPs/PABA/ERGO electrode, the current magnitude significantly decreased and ΔE_p increased to 250 mV (curve c), the behavior that seems to be directly related to the presence of the negatively charged phosphates groups in the backbone of DNA. In the final stage, the treatment of the fabricated biosensor toward 5 μL of 1 fM of the target DNA for 60 min further decreased the peak current and increased the ΔE_p value to 390 mV (curve d), which are in agreement with the above mentioned EIS results. In brief, the EIS and CV results made it clear that we succeeded the construction of an excellent nanocomposite platform, without sacrificing the interfacial conductivity of platform, for establishing a powerful DNA biosensor for monitoring of HIV-1 pol gene. As we have fully described in computational section 3.3, with employing this sandwiched structure, it is possible to quantify a sub-femtomolar

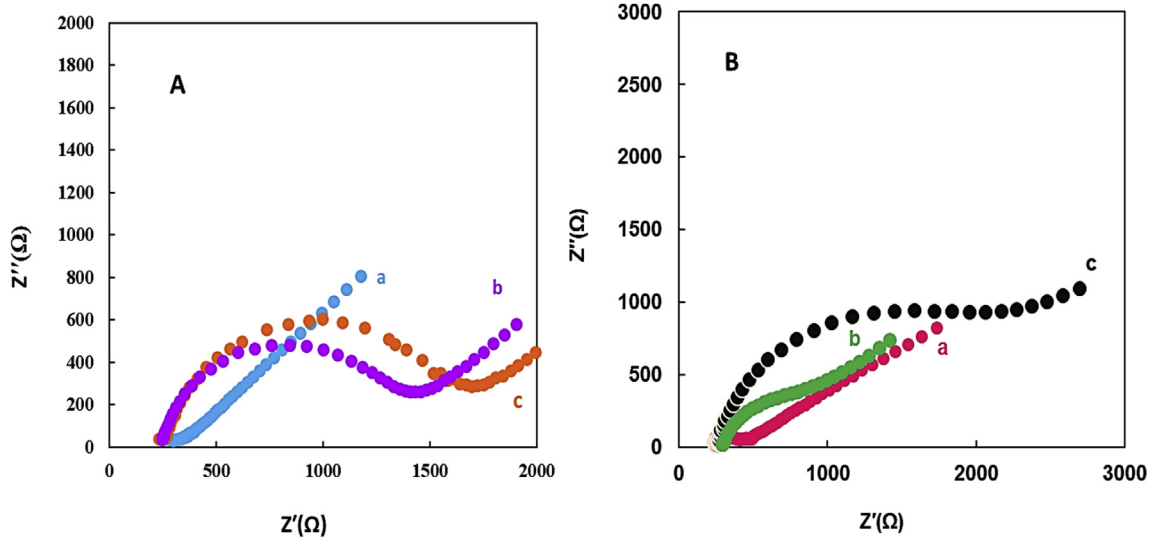

Fig. 4. (A) The Nyquist plots obtained with AuNPs/GCE (a), ssDNA/AuNPs/GCE (b), dsDNA/AuNPs/GCE (c), and (B) Nyquist diagrams obtained with AuNPs/PABA/GCE (a), ssDNA/AuNPs/PABA/GCE (b), dsDNA/AuNPs/PABA/GCE for 0.1 pM of target DNA in the solution of 5 mM of $[Fe(CN)6]^{3-/4-}$ solution containing 0.1 M KCl over frequency range of 10^5 to 0.01 Hz with $E_{ac} = 10$ mV.

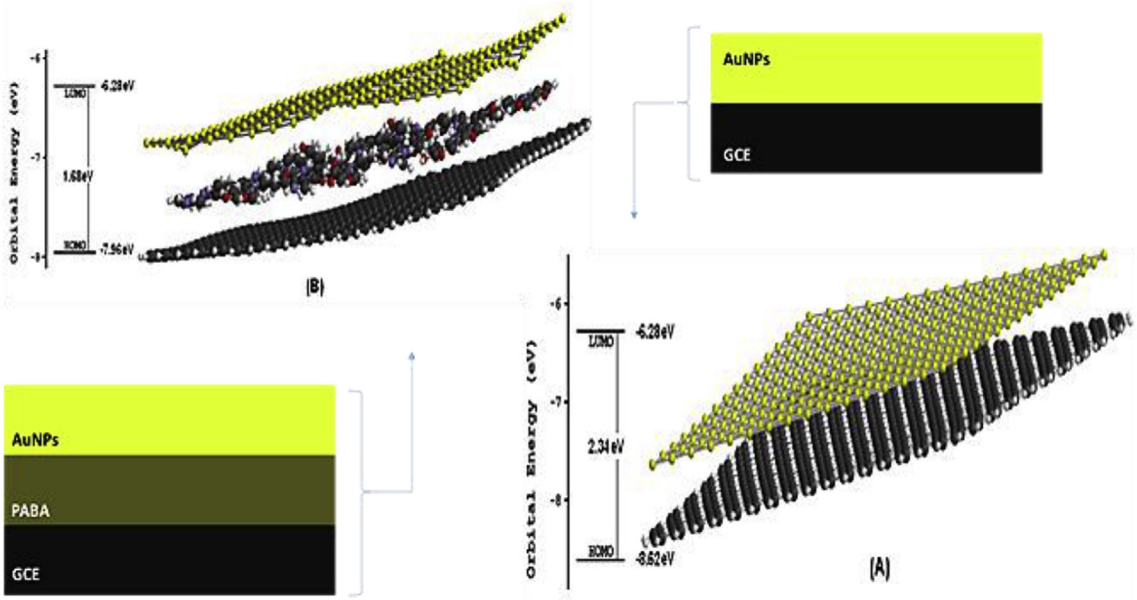

Fig. 5. The HOMO & LUMO energy levels and ΔEHOMO-LUMO gaps for two-layered Graphene-Au (A) and three-layered Graphene-PABA-Au (B).

amount of HIV-1 pol gene without any amplification or application of complicated detection schemes.

3.3. Computational methods and discussions

The theoretical results of the modeling of both arrayed composites including; the two layers model (form-A: Graphene-Au) and three layers model (form-B: Graphene-Polymer-Au) were performed with quantum mechanics (QM) and molecular mechanics (MM) appropriately. All of the calculations were performed using the *Spartan '10* package. For this modeling, each of the graphene, Au and polymer layers were first separately modeled and optimized, and based on the results obtained, the graphene-Au and graphene-polymer-Au models were calculated by molecular mechanics MMFF94 method. Then, the corresponding HOMO, LUMO and the HOMO-LUMO gaps ($\Delta E_{HOMO\text{-}LUMO}$) were calculated by UHF/PM6 (as a hybrid of *ab-initio* and semi-empirical QM methods) and the results are shown in Fig. 5. Here the graphene surface is shown by the ball and spoke model. The dimensions of the quadrangle graphene and Au were selected as 38.84×38.84 and 37.93×37.93 Å, respectively. It should be noted that, in the form-B (Graphene-Polymer-Au), the polymer chains are supported to place beside each other via possible hydrogen bonding between the amide functional groups [45], as noticed in Fig. S7. The results of calculation revealed that the Au layer in the form-A is *ca.* 60 kcal mol^{-1} more stable than the form-B (Figures not shown), so that the form-B should have more willingness to react with the DNA-SH (with −SH tail of the selected DNA). Due to its complexation with polymer layer [43], the Au layer in the form-B exhibited some distortions, compared with that in the form-A. These differences between the structures of two interfacial Au layers in the forms A and B can reasonably interpret the observed electrical resistance in experimental results. In other words, with the equal time of dipping of the composite electrode in the solution of probe DNA, it seems that the form-B provides a higher chance for successful complexation (chemisorption process) between the Au layer and SH-DNA. We believe that this characteristic can be mentioned as one of the main reasons that interpret the supreme sensitivity of the ssDNA/AuNPs/PABA/ERGO/GCE compared to the ssDNA/AuNPs/ERGO/GCE.

Fig. 5 shows the HOMO and LUMO energy levels and the $\Delta E_{HOMO\text{-}LUMO}$ energy gaps for both A and B forms. As is obvious, the energy levels of the HOMO and LUMO orbitals were calculated to be [-8.62 & −6.28] for the form-A and [-7.96 & −6.28] eV for the form-B and the corresponding HOMO-LUMO energy gaps are 2.34 eV and 1.68 eV, respectively. The results show that, due to the more bonding molecular orbitals and the repulsion between them, the HOMO energy level in the form-B is higher (more stable) than that in the form-A. These results caused smaller (0.66 eV) $\Delta E_{HOMO\text{-}LUMO}$ gap for the form-B compared to the form-A. Apart from the above-mentioned reason for the supreme behavior of the extended biosensor, it seems that the HOMO energy level changes and correspondingly the obtained $\Delta E_{HOMO\text{-}LUMO}$ gaps can be appropriately accepted as one of the rational reasons for the more sensitivity and reactivity observed for the form-B. It was generally accepted that the electrochemical properties, kinetic stability, hardness-softness and reactivity willingness are directly dependent on the HOMO and LUMO energy level orbitals and $\Delta E_{HOMO\text{-}LUMO}$ energy gaps [29,46,47].

3.4. Effect of incubation time

The effect of DNA hybridization time was investigated over the range of 5–90 min in the solution of 1 pM of the target. As is shown in Fig. S8, the maximum change in the analytical signal was obtained after the incubation time of 60 min. For longer times, R_{et} value did not significantly change, indicating that the ss-DNA probes on the modified electrode are completely hybridized by target DNA. Therefore, the hybridization of probe DNA and target DNA was accomplished through the incubation time of 60 min.

3.5. Analytical performance of the biosensor

The quantitative behavior of the fabricated biosensors toward HIV-1 pol gene was considered using EIS. The corresponding equivalent R_{et} was estimated from each Nyquist plot and a complete calibration curve was sketched against the concentration of HIV gene. Fig. 6A and B illustrate the Nyquist plots and the

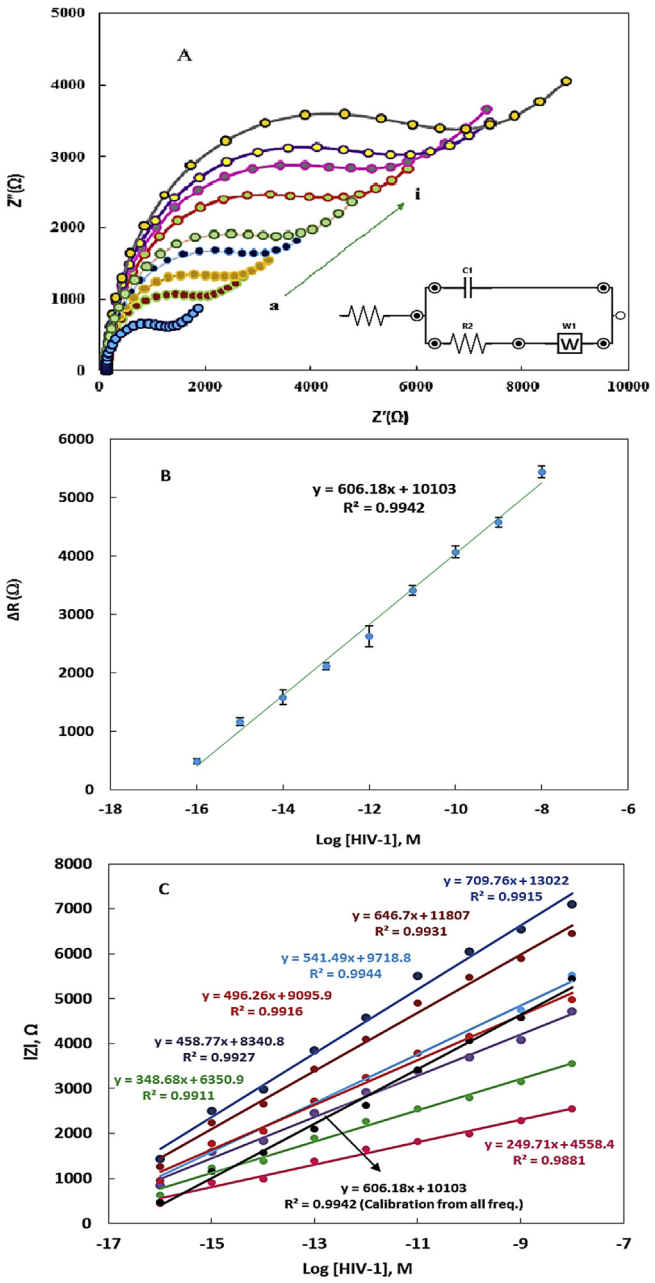

Fig. 6. (A) Nyquist plots of impedance spectra of the DNA biosensor for different concentrations of HIV-1 gene for 60 min: (a) 1.0×10^{-16} M, (b) 5.0×10^{-15} M, (c) 1.0×10^{-14} M, (d) 5.0×10^{-13} M, (e) 1.0×10^{-12} M, (f) 5.0×10^{-11} M, (g) 1.0×10^{-10} M, (h) 1.0×10^{-9} M, (i) 1.0×10^{-8} M. (B) The plot of ΔR_{et} (Ω) vs. log [HIV-1]. (C) Variation of total impedance (|Z|) as a function of log [HIV^{-1}] at different individual frequencies in relatively low frequency region.

corresponding calibration plot i. e. the logarithmic relationship between ΔR_{et} ($\Delta R_{et} = R_{et,dsDNA}$-$R_{et,ssDNA}$) and the concentration of the HIV-1 pol gene, respectively. The results appropriately disclose the increases of R_{et} with increasing the concentrations of complementary target DNA over the concentration range of 1.0×10^{-16} to 1.0×10^{-8} M. The regression equation was as $\Delta R_{et} = 606.18 \log (C/M) + 10103$ with a regression coefficient of 0.9942. The limit of detection found to be 3.7×10^{-17} M (at a S/N = 3). Alternatively, we also exploited a single frequency measurement (SFM) by recording the total impedance (|Z|) in each individual frequency, instead of recording one complete spectrum, which needs much longer time [26,48]. Practically, the variation of total impedance (|Z|) as a function of HIV gen at several frequencies, over the low frequencies' region, were sketched (Fig. 6C). Therefore, a calibration curve with comparable sensitivity can be constructed by measuring only one |Z| value for each concentration. Utilizing this alternative strategy in this work lead to a considerable saving in time together with easy functioning.

Table 1 shows the comparison of the dynamic linear range and limit of detection assessed by the proposed biosensor with those obtained by some of the best previously reported electrochemical biosensors for detection of HIV gene [8,9,49–54]. As clearly seen, apart from the dynamic linear range and limit of detection obtained by Wang et al. (reference 45) that are comparable with this work, the present biosensing system covers a much broader linear range and detect much lower amounts of HIV gene, compared with other published reports.

3.6. Selectivity, reproducibility and real sample analysis

To investigate that the developed biosensor could sufficiently distinguish the target DNA, the ssDNA/AuNPs/PABA/ERGO platform was reacted with target DNA and also three mismatched DNAs (double-base mismatched DNA, four-base mismatched DNA, and non-complementary DNA) at the same concentrations, respectively. As the results are shown in Fig. 7, the ΔR_{et} values were to be 44.51%, 23.03% and 5.21% of that observed for hybridization with the target DNA, for double base mismatched, four-base mismatched and non-complementary sequences, respectively. Indeed, the superior hybridization with the complementary sequences effectively affects the interfacial properties compared to the case of mismatched sequences. By increasing the mismatched sequences, the interference with the main hybridization process increased, which causes less double helix formation and lower signal intensity.

To evaluate the reproducibility of the DNA sensor, five sensors were fabricated to independently detect 1 pM of target DNA under the same experimental conditions. The relative standard deviation (RSD) based on five independent measurements was 5.94%. These experimental results indicated that the proposed sensor has good reproducibility. The results of three successive determinations of 1 pM of target DNA with a single modified electrode under the same conditions resulted in an RSD 2.7%. The corresponding impedance curves are shown in Fig. S9. The capability of the DNA biosensor for the detection of the target in real samples was studied. For this purpose, we used standard addition method with the spiked different concentration of HIV DNA in human serum sample that was diluted (100-fold) with phosphate buffer solution (pH = 7.4). Each sample was analyzed three times and the corresponding results are shown in Table 2, which discloses a good recovery in real serum samples. Therefore, the impedimetric DNA biosensor can be used to determine HIV gene in serum samples.

4. Conclusion

Contrary to almost all biosensing works, and contrary to our previous works [26,28,55] that by nanomaterials, where, mostly the change of diffusion regime and the increase of surface-to-volume was the main reason for signal strengthening, here, we accomplish notable signal-amplifying via the change of electrical properties of the composite. The present study introduces a simple impedimetric DNA biosensor by employing a new easily constructed sandwich nanocomposite film with the capability of monitoring sub-femtomolar concentration of HIV-1 pol gene. The ssDNA/AuNPs/PABA/ERGO/GCE revealed a supreme sensitivity toward HIV-1 pol gene compared to ssDNA/AuNPs/ERGO/GCE, just because sandwiching PABA conducting polymer between ERGO

Table 1
Comparison of the dynamic linear range (DLR) and limit of detection (LOD) of the proposed biosensing system with those of previously reported electrochemical biosensors for HIV-1 gene.

Type of biosensor	Technique	DLR (M)	LOD (M)	Ref.
Label-free Au-IL/PTCA/GR modified electrode	EIS	$1.0 \times 10^{-13} - 1.0 \times 10^{-6}$	3.4×10^{-14}	[51]
Methylene blue as a hybridization redox indicator	SWV	$2.0 \times 10^{-8} - 1.0 \times 10^{-7}$	1.0×10^{-10}	[9]
Exo III/AuNCs/GR/GCE	DPV	$1.0 \times 10^{-16} - 1.0 \times 10^{-7}$	3.0×10^{-17}	[54]
Au–Ag-PPy modified platinum electrode	EIS	$1.0 \times 10^{-9} - 1.0 \times 10^{-6}$	5.0×10^{-10}	[49]
Label-free GR-Nafion composite film modified electrode	EIS	$1.0 \times 10^{-13} - 1.0 \times 10^{-10}$	2.3×10^{-14}	[8]
Label-free ERGO-modified electrode	EIS	$1.0 \times 10^{-12} - 1.0 \times 10^{-6}$	1.0×10^{-13}	[50]
3,4,9,10-Perylene tetracarboxylic acid functionalized graphene modified electrode	EIS	$1.0 \times 10^{-12} - 1.0 \times 10^{-6}$	5.5×10^{-13}	[52]
GO anchored on a diazonium functionalized electrode	EIS	$1.0 \times 10^{-12} - 1.0 \times 10^{-6}$	1.1×10^{-13}	[53]
AuNPs/4-PABA/ERGO/GCE	EIS	$1.0 \times 10^{-16} - 1.0 \times 10^{-7}$	3.7×10^{-17}	This work

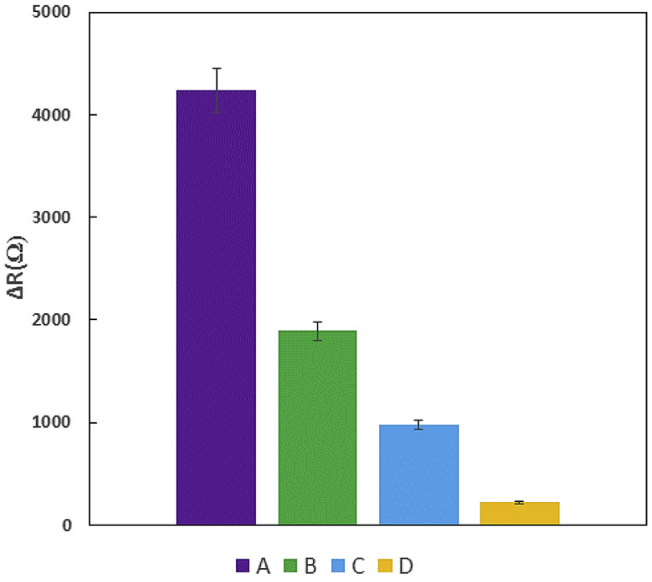

Fig. 7. Comparison of hybridization signal intensities for pDNA immobilized AuNPs/PABA/ERGO platform hybridized with target DNA (a), double-base mismatched DNA (b), four-base mismatched (c) and non-complementary sequences (d). The detection concentrations of these sequences were all selected as 1.0×10^{-10} M.

Table 2
Detection of HIV DNA in the spiked human serum sample.

Sample	Added	Found	Recovery (%)	RSD (%)
1	10 fM	9.33 fM	93.3	5.87
2	10 nM	9.68 nM	96.8	5.65

sub-layer and AuNPs interfacial layer. The DFT calculation results confirmed the supreme influence of PABA located beside the AuNPs in providing a different surface with exclusive effect on electronic characteristics of the platform as a transducer. A single frequency measurement was also employed to reduce the measurement time. The above mentioned strategies aided us to attain a sensitive and repeatable analytical response toward HIV-1 pol gene without using any amplification strategy. Such studies would more help us to establish new composites with superior transducing properties in sensing devices, as is currently the subject of our research group's attempts.

Declaration of interests

The authors declare that they have no known competing financial interests or personal relationships that could have appeared to influence the work reported in this paper.

Appendix A. Supplementary data

Supplementary data to this article can be found online at https://doi.org/10.1016/j.aca.2018.12.013.

References

[1] I. Berkower, G.E. Smith, C. Giri, D. Murphy, Human immunodeficiency virus 1. Predominance of a group-specific neutralizing epitope that persists despite genetic variation, J. Exp. Med. 170 (1989) 1681–1695.
[2] A. Bhimji, A.A. Zaragoza, L.S. Live, S.O. Kelley, Electrochemical enzyme-linked immunosorbent assay featuring proximal reagent generation: detection of human immunodeficiency virus antibodies in clinical samples, Anal. Chem. 85 (2013) 6813–6819.
[3] B.M. Cerrutti, M.L. Moraes, S.H. Pulcinelli, C.V. Santilli, Lignin as immobilization matrix for HIV p17 peptide used in immunosensing, Biosens. Bioelectron. 71 (2015) 420–426.
[4] S. Horiya, J.K. Bailey, J.S. Temme, Y.V. Guillen Schlippe, I.J. Krauss, Directed evolution of multivalent glycopeptides tightly recognized by HIV antibody 2G12, J. Am. Chem. Soc. 136 (2014) 5407–5415.
[5] J. Liu, B. Du, P. Zhang, M. Haleyurgirisetty, J. Zhao, V. Ragupathy, S. Lee, D.L. DeVoe, I.K. Hewlett, Development of a microchip Europium nanoparticle immunoassay for sensitive point-of-care HIV detection, Biosens. Bioelectron. 61 (2014) 177–183.
[6] P.M. Martínez, A.R. Torres, R.O. de Lejarazu, A. Montoya, J.F. Martín, J.M. Eiros, Human immunodeficiency virus antibody testing by enzyme-linked fluorescent and western blot assays using serum, gingival-crevicular transudate, and urine samples, J. Clin. Microbiol. 37 (1999) 1100–1106.
[7] J. Shu, Z. Qiu, S. Lv, K. Zhang, D. Tang, Plasmonic enhancement coupling with defect-engineered TiO2–x: a mode for sensitive photoelectrochemical biosensing, Anal. Chem. 90 (2018) 2425–2429.
[8] Q. Gong, Y. Wang, H. Yang, A sensitive impedimetric DNA biosensor for the determination of the HIV gene based on graphene-Nafion composite film, Biosens. Bioelectron. 89 (2017) 565–569.
[9] D. Zhang, Y. Peng, H. Qi, Q. Gao, C. Zhang, Label-free electrochemical DNA biosensor array for simultaneous detection of the HIV-1 and HIV-2 oligonucleotides incorporating different hairpin-DNA probes and redox indicator, Biosens. Bioelectron. 25 (2010) 1088–1094.
[10] S. Zhang, K. Wang, K.-B. Li, W. Shi, W.-P. Jia, X. Chen, T. Sun, D.-M. Han, A DNA-stabilized silver nanoclusters/graphene oxide-based platform for the sensitive detection of DNA through hybridization chain reaction, Biosens. Bioelectron. 91 (2017) 374–379.
[11] E. Albers, M. Sbroggiò, J. Martin-Gonzalez, A. Avram, S. Munk, A.J. Lopez-Contreras, A simple DNA recombination screening method by RT-PCR as an alternative to Southern blot, Transgenic Res. 26 (2017) 429–434.
[12] J. Compton, Nucleic acid sequence-based amplification, Nature 350 (1991) 91–92.
[13] J. Li, T. Deng, X. Chu, R. Yang, J. Jiang, G. Shen, R. Yu, Rolling circle amplification combined with gold nanoparticle aggregates for highly sensitive identification of single-nucleotide polymorphisms, Anal. Chem. 82 (2010) 2811–2816.
[14] F. Li, J. Han, L. Jiang, Y. Wang, Y. Li, Y. Dong, Q. Wei, An ultrasensitive sandwich-type electrochemical immunosensor based on signal amplification strategy of gold nanoparticles functionalized magnetic multi-walled carbon nanotubes loaded with lead ions, Biosens. Bioelectron. 68 (2015) 626–632.
[15] R. Malhotra, V. Patel, J.P. Vaqué, J.S. Gutkind, J.F. Rusling, Ultrasensitive electrochemical immunosensor for oral cancer biomarker IL-6 using carbon nanotube forest electrodes and multilabel amplification, Anal. Chem. 82 (2010) 3118–3123.
[16] Q. Zhou, Y. Lin, K. Zhang, M. Li, D. Tang, Reduced graphene oxide/BiFeO3 nanohybrids-based signal-on photoelectrochemical sensing system for prostate-specific antigen detection coupling with magnetic microfluidic

device, Biosens. Bioelectron. 101 (2018) 146–152.
[17] M.A. Bangar, D.J. Shirale, W. Chen, N.V. Myung, A. Mulchandani, Single conducting polymer nanowire chemiresistive label-free immunosensor for cancer biomarker, Anal. Chem. 81 (2009) 2168–2175.
[18] J. Shu, Z. Qiu, D. Tang, Self-referenced smartphone imaging for visual screening of H2S using Cu x O-polypyrrole conductive aerogel doped with graphene oxide framework, Anal. Chem. 90 (2018) 9691–9694.
[19] J.F. Mike, J.L. Lutkenhaus, Recent advances in conjugated polymer energy storage, J. Polym. Sci. B: Pol. Phys. 51 (2013) 468–480.
[20] A. Malinauskas, Electrocatalysis at conducting polymers, Synth. Met. 107 (1999) 75–83.
[21] A.S. Widge, M. Jeffries-El, X. Cui, C.F. Lagenaur, Y. Matsuoka, Self-assembled monolayers of polythiophene conductive polymers improve biocompatibility and electrical impedance of neural electrodes, Biosens. Bioelectron. 22 (2007) 1723–1732.
[22] K.-J. Huang, C.-X. Xu, W.-Z. Xie, W. Wang, Electrochemical behavior and voltammetric determination of tryptophan based on 4-aminobenzoic acid polymer film modified glassy carbon electrode, Colloids Surfaces B Biointerfaces 74 (2009) 167–171.
[23] M. Wang, W. Gong, Q. Meng, Y. Zhang, Electrochemical DNA impedance biosensor for the detection of DNA hybridization with polymeric film, single walled carbon nanotubes modified glassy carbon electrode, Russ. J. Electrochem. 47 (2011) 1368–1373.
[24] Y. Zhang, J. Wang, M. Xu, A sensitive DNA biosensor fabricated with gold nanoparticles/ploy (p-aminobenzoic acid)/carbon nanotubes modified electrode, Colloids Surfaces B Biointerfaces 75 (2010) 179–185.
[25] W. Zhu, H. Huang, X. Gao, H. Ma, Electrochemical behavior and voltammetric determination of acetaminophen based on glassy carbon electrodes modified with poly (4-aminobenzoic acid)/electrochemically reduced graphene oxide composite films, Mater. Sci. Eng. C 45 (2014) 21–28.
[26] M. Shamsipur, A. Pashabadi, F. Molaabasi, S. Hosseinkhani, Impedimetric monitoring of apoptosis using cytochrome-aptamer bioconjugated silver nanocluster, Biosens. Bioelectron. 90 (2017) 195–202.
[27] M. Shamsipur, A. Pashabadi, A.A. Taherpour, K. Bahrami, H. Sharghi, Manganese mediated oxidation of progesterone in alkaline medium: mechanism study and quantitative determination, Electrochim. Acta 225 (2017) 292–302.
[28] M. Shamsipur, A. Pashabadi, A.A. Taherpour, B. Hemmateenejad, T. Khosousi, M.H. Parvin, Synthesis and characterization of glucose-capped CdSe quantum dots. Electrochemical and computational studies of corresponding carbon-ionic liquid electrode for quantitative determination of minoxidil, J. Electroanal. Chem. 778 (2016) 116–125.
[29] M. Shamsipur, A.A. Taherpour, A. Pashabadi, Interrupting the flux of delocalized electrons on a dibenzo-18-crown-6-embedded graphite sheet and its relative counteraction in the presence of potassium ions, Analyst 141 (2016) 4227–4234.
[30] M. Shamsipur, A.A. Taherpour, H. Sharghi, A. Pashabadi, Transduction of interaction between trace tryptophan and surface-confined chromium salen using impedance spectroscopy. A sensing device that works based on highly selective inhibition of mediator's Faradaic process, Anal. Chim. Acta 1030 (2018) 70–76.
[31] M. Shamsipur, A. Taherpour, A. Pashabadi, Comprehensive facilitating of water oxidation reaction by ultrasonic attenuation of hydrogen-bonded structure of water, Ultrason. Sonochem. 42 (2018) 381–389.
[32] M. Shamsipur, A.A. Taherpour, H. Sharghi, V. Lippolis, A. Pashabadi, A low-overpotential nature-inspired molecular chromium water oxidation catalyst, Electrochim. Acta 265 (2018) 316–325.
[33] W.S. Hummers Jr., R.E. Offeman, Preparation of graphitic oxide, J. Am. Chem. Soc. 80 (1958), 1339-1339.
[34] N.I. Kovtyukhova, P.J. Ollivier, B.R. Martin, T.E. Mallouk, S.A. Chizhik, E.V. Buzaneva, A.D. Gorchinskiy, Layer-by-layer assembly of ultrathin composite films from micron-sized graphite oxide sheets and polycations, Chem. Mater. 11 (1999) 771–778.
[35] M. Shamsipur, L. Farzin, M.A. Tabrizi, F. Molaabasi, Highly sensitive label free electrochemical detection of VGEF165 tumor marker based on “signal off” and “signal on” strategies using an anti-VEGF165 aptamer immobilized BSA-gold nanoclusters/ionic liquid/glassy carbon electrode, Biosens. Bioelectron. 74 (2015) 369–375.
[36] Y. Zhang, G. Jin, W. Cheng, S. Li, Poly (O-aminobenzoic acid) modified glassy carbon electrode for electrochemical detection of dopamine in the presence of ascorbic acid, Front. Biosci. 10 (2005) 23–29.
[37] P. Khanra, T. Kuila, N.H. Kim, S.H. Bae, D.-s. Yu, J.H. Lee, Simultaneous bifunctionalization and reduction of graphene oxide by baker's yeast, Chem. Eng. J. 183 (2012) 526–533.
[38] Z. Luo, Y. Lu, L.A. Somers, A.C. Johnson, High yield preparation of macroscopic graphene oxide membranes, J. Am. Chem. Soc. 131 (2009) 898–899.
[39] S. Stankovich, D.A. Dikin, R.D. Piner, K.A. Kohlhaas, A. Kleinhammes, Y. Jia, Y. Wu, S.T. Nguyen, R.S. Ruoff, Synthesis of graphene-based nanosheets via chemical reduction of exfoliated graphite oxide, Carbon 45 (2007) 1558–1565.
[40] P. Wen, X. Wang, Synthesis and visible photocatalytic activities of poly (aminobenzoic acid)/TiO 2 nanocomposites, J. Nanomater. 2013 (2013) 161.
[41] M. Samsonowicz, T. Hrynaszkiewicz, R. Świsłocka, E. Regulska, W. Lewandowski, Experimental and theoretical IR, Raman, NMR spectra of 2-, 3-and 4-aminobenzoic acids, J. Mol. Struct. 744 (2005) 345–352.
[42] M. Zhou, Y. Zhai, S. Dong, Electrochemical sensing and biosensing platform based on chemically reduced graphene oxide, Anal. Chem. 81 (2009) 5603–5613.
[43] P. Buduru, Oxamic acid and p-aminobenzoic acid functionalized gold nanoparticles as a probe for colorimetric detection of Fe3+ ion, Sens. Actuators B-Chem. 237 (2016) 935–943.
[44] A.J. Bard, L.R. Faulkner, Fundamentals and applications, Electrochem. Meth. 2 (2001) 482.
[45] Y. Shibasaki, Y. Abe, N. Sato, A. Fujimori, Y. Oishi, Direct condensation polymerization of N-alkylated p-aminobenzoic acid and packing of rigid-rod main chains with flexible side chains, Polym. J. 42 (2010) 72.
[46] D. Music, R.W. Geyer, J.M. Schneider, Recent progress and new directions in density functional theory based design of hard coatings, Surf. Coating. Technol. 286 (2016) 178–190.
[47] A.A. Taherpour, Theoretical and quantitative structural relationship study of the electrochemical properties of [M2@ C x]@[SWCNT (5, 5)-Armchair-C n H20](M= Er and Sc, x= 82 and 84, and n= 20– 300) complexes, J. Phys. Chem. C 113 (2009) 5402–5408.
[48] E. Katz, L. Alfonta, I. Willner, Chronopotentiometry and Faradaic impedance spectroscopy as methods for signal transduction in immunosensors, Sens. Actuators B-Chem. 76 (2001) 134–141.
[49] Y. Fu, R. Yuan, Y. Chai, L. Zhou, Y. Zhang, Coupling of a reagentless electrochemical DNA biosensor with conducting polymer film and nanocomposite as matrices for the detection of the HIV DNA sequences, Anal. Lett. 39 (2006) 467–482.
[50] Q. Gong, H. Yang, Y. Dong, W. Zhang, A sensitive impedimetric DNA biosensor for the determination of the HIV gene based on electrochemically reduced graphene oxide, Anal. Methods 7 (2015) 2554–2562.
[51] Y. Hu, S. Hua, F. Li, Y. Jiang, X. Bai, D. Li, L. Niu, Green-synthesized gold nanoparticles decorated graphene sheets for label-free electrochemical impedance DNA hybridization biosensing, Biosens. Bioelectron. 26 (2011) 4355–4361.
[52] Y. Hu, F. Li, X. Bai, D. Li, S. Hua, K. Wang, L. Niu, Label-free electrochemical impedance sensing of DNA hybridization based on functionalized graphene sheets, Chem. Commun. 47 (2011) 1743–1745.
[53] Y. Hu, F. Li, D. Han, T. Wu, Q. Zhang, L. Niu, Y. Bao, Simple and label-free electrochemical assay for signal-on DNA hybridization directly at undecorated graphene oxide, Anal. Chim. Acta 753 (2012) 82–89.
[54] Y. Wang, X. Bai, W. Wen, X. Zhang, S. Wang, Ultrasensitive electrochemical biosensor for HIV gene detection based on graphene stabilized gold nanoclusters with exonuclease amplification, ACS Appl. Mater. Interfaces 7 (2015) 18872–18879.
[55] M. Shamsipur, A. Pashabadi, F. Molaabasi, A novel electrochemical hydrogen peroxide biosensor based on hemoglobin capped gold nanoclusters–chitosan composite, RSC Adv. 5 (2015) 61725–61734.